M. C. Teich, C. Heneghan, S. B. Lowen, and R. G. Turcott, in Wavelets in Medicine and Biology, edited by A. Aldroubi and M. Unser (CRC Press, Boca Raton, 1996), ch. 14, pp. 383-412.

14

Estimating the Fractal Exponent of Point Processes in Biological Systems Using Wavelet- and Fourier-Transform Methods

Malvin C. Teich,[1,2,3] Conor Heneghan,[1,3] Steven B. Lowen,[3] and Robert G. Turcott[3,4]

[1] *Department of Electrical, Computer & Systems Engineering, Boston University, Boston;*
[2] *Department of Biomedical Engineering, Boston University, Boston;*
[3] *Department of Electrical Engineering, Columbia University, New York;*
[4] *School of Medicine, Stanford University, Palo Alto, California.*

14.1 Introduction

Some random phenomena occur at discrete times or locations, with the individual events largely identical, such as the detection of particles from radioactive decay. A stochastic point process [8] is a mathematical construction which represents these events as random points in a space. Such a process may be called fractal when a number of the relevant statistics of the point process exhibit scaling with related scaling exponents, indicating that the represented phenomenon contains clusters of points over all (or a relatively large set of) time or length scales. In this chapter, we consider point processes on a line, which model a variety of observed phenomena in the biological sciences.

M. C. Teich, C. Heneghan, S. B. Lowen, and R. G. Turcott, in Wavelets in Medicine and Biology, edited by A. Aldroubi and M. Unser (CRC Press, Boca Raton, 1996), ch. 14, pp. 383-412.

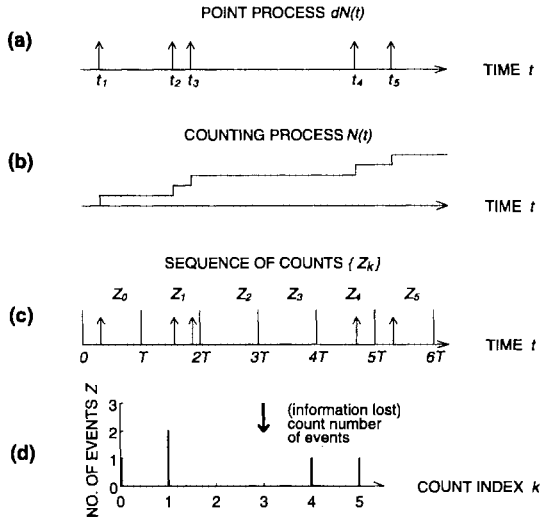

Figure 14.1
Representations of a point process. (a) The events are represented by a sequence of idealized impulses, occurring at times t_k, and forming a stochastic point process $dN(t)$. For convenience of analysis, several alternative representations of the point process are used. (b) The counting process $N(t)$. At every event occurrence the value of $N(t)$ augments by unity. (c) The sequence of counts $\{Z_k\}$, a discrete-time, nonnegative integer-valued stochastic process, is formed from the point process by recording the number of events in successive counting windows of length T. (d) The sequence of counts $\{Z_k\}$ can be conveniently described in terms of a count index k. Information is lost because the precise times of event occurrences within each counting window are eliminated in this representation. Correlations in the discrete-time sequence $\{Z_k\}$ can be readily interpreted in terms of real time.

14.1.1 Mathematical Descriptions of Stochastic Point Processes

Figure 14.1 shows several representations that are useful in the analysis of point processes. Figure 14.1(a) demonstrates the modeling of a point process as a series of impulses occurring at specified times t_k. Since these impulses have vanishing width, they are most rigorously defined as the derivative of a well-defined counting process $N(t)$ (Figure 14.1[b]), a monotonically increasing function of t, that augments by unity when an event occurs. Accordingly, the point process itself is properly written as $dN(t)$, since it is only strictly defined within the context of an integral.

The point process is completely described by the set of event times $\{t_k\}$, or equivalently by the set of interevent intervals. However, the sequence of

M. C. Teich, C. Heneghan, S. B. Lowen, and R. G. Turcott, in Wavelets in Medicine and Biology, edited by A. Aldroubi and M. Unser (CRC Press, Boca Raton, 1996), ch. 14, pp. 383-412.

counts depicted in Figure 14.1(c) also contains much information about the process. Here the time axis is divided into equally sized contiguous counting windows of length T seconds to produce a sequence of counts $\{Z_k\}$, where $Z_k = N[(k+1)T] - N[kT]$ denotes the number of events in the kth window. As illustrated in Figure 14.1(d), this sequence forms a discrete-time random process of nonnegative integers. In general, information is lost in forming the sequence of counts, although for a regular point process the amount lost can be made arbitrarily small by reducing the size of the counting window T. An attractive feature of this representation is that it preserves the correspondence between the discrete time axis of the counting process $\{Z_k\}$ and the absolute "real" time axis of the underlying point process. Within the process of counts $\{Z_k\}$, the elements Z_k and Z_{k+n} refer to the number of counts in windows separated by precisely $T(n-1)$ seconds, so that correlation in the process $\{Z_k\}$ is readily associated with correlation in the underlying point process $dN(t)$.

14.1.2 Fractal Stochastic Point Processes (FSPPs) Exhibit Scaling

The characterization of a stochastic process involves a complete description of all possible joint probabilities of the various events occurring in the process. Different statistics provide complementary views of the process; no single statistic can in general describe a stochastic process completely. We call a stochastic point process *fractal* if it exhibits scaling in many of its statistics. Such scaling leads naturally to power-law behavior, as demonstrated in the following. Consider a statistic f which depends continuously on the scale x over which measurements are taken. Suppose changing the scale by a factor a effectively multiplies the statistic by some other factor $g(a)$, related to the factor but independent of the scale:

$$f(ax) = g(a)f(x). \tag{14.1}$$

The only nontrivial solution of this scaling equation is

$$f(x) = bg(x) \quad \text{with } g(x) = x^c \tag{14.2}$$

for some constants b and c [22, 26]. Thus, statistics with power-law forms are closely related to this concept of a fractal.

For example, consider a commonly encountered first-order statistic for a stochastic point process, the interevent interval histogram (IIH). This estimates the interevent-interval probability density function (IIPDF) $p(t)$ by computing the relative frequency of occurrence of interevent intervals as a function of interval size. This measure highlights the behavior of the times

M. C. Teich, C. Heneghan, S. B. Lowen, and R. G. Turcott, in Wavelets in Medicine and Biology, edited by A. Aldroubi and M. Unser (CRC Press, Boca Raton, 1996), ch. 14, pp. 383-412.

between adjacent events, but reveals none of the information contained in the relationships among these times, such as correlation between adjacent time intervals. For a fully fractal point process, the IIPDF follows the form of Equation 14.2, so that $p(t) \sim t^c$ over a certain range of t, where $c < -1$.

A number of statistics may be used to describe an FSPP, and each statistic which scales will, in general, have a different scaling exponent c. Each of these exponents can be simply related to a more general parameter α, the fractal exponent, where the exact relation between these two exponents will depend upon the statistic in question. For example, the exponent c of the IIPDF defined above can be related to the fractal exponent α by $c = -(1 + \alpha)$.

The fractal exponent α defined above is also related to the more commonly encountered Hurst exponent H [24, 29]. The relationship is ambiguous, however, since some authors [11–13, 24, 41] use the formula $\alpha = 2H+1$ for all values of α, while others [5] use $\alpha = 2H - 1$ for $\alpha < 1$ to restrict H to the range $(0, 1)$. In this chapter, we avoid this confusion by considering α directly instead of H.

14.1.3 The Standard Fractal Renewal Process

Comparing existing methods of estimating the fractal exponent of point processes with techniques based on wavelets requires a benchmark fractal stochastic point process. Perhaps the most easily described FSPP is the standard fractal renewal process (SFRP) [7, 18, 19, 20, 23]; we focus on this process because of its relative ease of analysis, its simple and straightforward simulation, and its usefulness in describing a variety of real-world processes.

For the SFRP, the times between adjacent events are independent random variables t drawn from the same fractal probability distribution. In particular, the IIPDF $p(t)$ decays essentially as a power law; we illustrate this with a particular form with abrupt cutoffs

$$p(t) = \frac{\alpha}{A^{-\alpha} - B^{-\alpha}} \begin{cases} t^{-(\alpha+1)} & \text{for } 0 < A < t < B \\ 0 & \text{otherwise,} \end{cases} \tag{14.3}$$

with α the fractal exponent and A and B cutoff parameters. The SFRP exhibits fractal behavior over timescales lying between A and B. This process is fully fractal: it exhibits scaling both in the IIPDF and in the second-order statistics that we discuss in Section 14.2.

M. C. Teich, C. Heneghan, S. B. Lowen, and R. G. Turcott, in Wavelets in Medicine and Biology, edited by A. Aldroubi and M. Unser (CRC Press, Boca Raton, 1996), ch. 14, pp. 383-412.

14.1.4 Examples of Fractal Stochastic Point Processes in Nature

Many phenomena are readily represented by FSPPs or by functions derived from them. We provide several examples drawn from the biological sciences. We have carried out similar analyses for physical phenomena such as trapping in semiconductors [18, 19] and noise and traffic in communication systems [27].

Biological Ion-Channel Openings

Ion channels reside in cell membranes, permitting ions to diffuse in or out [28]. These channels are usually specific to a particular ion, or group of related ions, and block the passage of other kinds of ions. Further, most channels have gates, and thus the channels may be either open or closed. In many instances, intermediate conduction states are not observed. Some ion channels may be modeled by a two-state Markov process [10], with one state representing the open channel and the other representing the closed channel. This model generates exponentially distributed dwell times in both states, which are, in fact, sometimes observed. However, many ion channels exhibit independent power-law-distributed closed times between open times of negligible duration [17] and are well described by an SFRP [20, 21, 30].

Auditory-Nerve-Fiber Action Potentials

Many biological neurons transmit information by means of action potentials, which are localized regions of depolarization traveling down the length of an axon. Action potentials on a given axon are brief and largely identical events, so their reception at another neuron (or at a recording electrode) may be well represented by a point process. FSPPs have been shown to describe the action potentials in primary auditory nerve fibers in a number of species [16, 30, 31, 33, 34]. Over short timescales, nonfractal stochastic point processes prove adequate for representing such nerve spikes, but over long timescales (typically greater than one second) fractal behavior becomes evident. Furthermore, estimators of the rate of the process converge more slowly than for nonfractal processes, displaying fluctuations which decrease as a power-law function of the time used to estimate the rate [32]. With the inclusion of the refractory effects of nerve fibers, an FSPP model can be shown to provide an excellent approximation for modeling the behavior of nerve spikes in auditory fibers in several species over all time scales and for a broad variety of statistical measures [16, 21, 31, 33, 34]; only four parameters are required. This process may well arise from superpositions of fractal ion channel transitions in inner ear sensory cells, as described briefly in the section on biological ion channel openings [20, 21].

M. C. Teich, C. Heneghan, S. B. Lowen, and R. G. Turcott, in Wavelets in Medicine and Biology, edited by A. Aldroubi and M. Unser (CRC Press, Boca Raton, 1996), ch. 14, pp. 383-412.

Visual-System Action Potentials

As with auditory nerve fibers, some neurons in the visual system transmit information by means of action potentials, and FSPPs provide suitable models for describing the behavior of these neurons [36]. The gamma renewal process, which is nonfractal, has proved to be a useful model for some of these processes over short timescales [37]. However, nerve spike trains recorded from both cat retinal ganglion cell and lateral geniculate nucleus neurons, like those recorded from primary auditory neurons, exhibit fractal behavior over timescales greater than one second, as will become apparent in Section 14.2. This necessitates the use of an FSPP model for these neural spike trains as well [36]. Similar fractal behavior has already been demonstrated for cat striate cortex neurons [35] and for an insect visual interneuron [39].

Human Heartbeat Times

The sequence of human heartbeats exhibits considerable variability over time and among individuals, both in the short-term and the long-term patterns of the beats. These effects can be studied by focusing on the times of maximum contraction, thus forming a point process of heartbeats. A particular FSPP, with an integrate-and-reset (rather than a Poisson) substrate, has been constructed and shown to successfully describe these events [38, 40]. In many respects the heartbeat process resembles the process formed by peripheral auditory and visual system action potentials. Over short timescales, nonfractal point processes provide suitable models for the pattern of times between contractions; for times longer than roughly 10 s, only fractal models suffice. Further, parameters of the FSPP used to model the data may have applicability for the diagnosis of various disease states [40].

14.2 Methods of Estimating the Fractal Exponent of Fractal Point Processes

As the examples described above illustrate, many natural phenomena are amenable to modeling by FSPPs. The value of the fractal exponent α can often provide important information regarding the nature of an underlying process, and can also serve as a useful classification tool (as indicated in the subsection pertaining to the human heartbeat above). Accordingly, it is desirable to estimate α reliably [29], although this task is often confounded by a variety of issues [6] (see [22] for a detailed discussion).

Here we briefly review some of the techniques used for estimating α. We show how two of these, the Fano and Allan factors, can be generalized

M. C. Teich, C. Heneghan, S. B. Lowen, and R. G. Turcott, in Wavelets in Medicine and Biology, edited by A. Aldroubi and M. Unser (CRC Press, Boca Raton, 1996), ch. 14, pp. 383-412.

as wavelet-based measures. To illustrate these techniques, we apply them to a train of action potentials recorded from a lateral geniculate nucleus (LGN) relay neuron in the cat visual system. There are 24,285 events in this particular spike train, with an average interevent interval of 0.132 s, comprising a total duration of 3225 s [36].

14.2.1 Coincidence Rate

The first measure we consider is the coincidence rate (CR). The CR measures the correlations between pairs of events with a specified time delay between them, regardless of intervening events, and is related to the autocorrelation function used with continuous processes. The CR is defined as

$$G(\tau) \equiv \lim_{\Delta \to 0} \frac{\Pr\{\mathcal{E}[0,\Delta] \text{ and } \mathcal{E}[\tau,\tau+\Delta]\}}{\Delta^2}, \tag{14.4}$$

where $\mathcal{E}[s,t]$ denotes the occurrence of at least one event of the point process in the interval $[s,t)$. For an ideal fractal point process the coincidence rate assumes the form [22]

$$G(\tau) = \lambda\delta(\tau) + \lambda^2\left[1 + (|\tau|/\tau_0)^{\alpha-1}\right], \tag{14.5}$$

where λ is the mean rate of the process, $\delta(\tau)$ denotes the Dirac delta function, τ_0 is a fractal onset time constant, and $0 < \alpha < 1$ is the fractal exponent.

The coincidence rate can be directly estimated from its definition. However, in practice the CR is a noisy measure, since its definition essentially involves a double derivative. Furthermore, for FSPPs typical of physical and biological systems, the CR exceeds its asymptotic value λ^2 at $\tau \to \infty$ by only a small fraction at any practical value of τ, so that determining the fractal exponent with this small excess presents serious difficulties. Therefore we do not specifically apply this measure to the LGN data, although the formal definition of coincidence rate plays a useful role in developing other, more reliable measures.

14.2.2 Power Spectral Density

The power spectral density (PSD) is a familiar and well-established measure for continuous-time processes. For point processes, the PSD and the CR introduced above form a Fourier transform pair, much like the PSD and the autocorrelation function do for continuous-time processes. The PSD provides a measure of how the power in a process is concentrated in various frequency bands. For a fractal point process, the PSD assumes the

M. C. Teich, C. Heneghan, S. B. Lowen, and R. G. Turcott, in Wavelets in Medicine and Biology, edited by A. Aldroubi and M. Unser (CRC Press, Boca Raton, 1996), ch. 14, pp. 383-412.

form

$$S(\omega) = \lambda \left[1 + (\omega/\omega_0)^{-\alpha}\right], \tag{14.6}$$

for relevant time and frequency ranges, where λ is the mean rate of events and ω_0 is a cutoff frequency.

The PSD of a point process can be estimated with the periodogram (PG) $S_N(\omega)$ of the sequence of counts, rather than from the point process itself [25]. This method introduces a bias at higher frequencies, since the fine time resolution information is lost as a result of the minimum-count window size. Nevertheless, since estimation of the fractal exponent principally involves lower frequencies where this bias is negligible, and employing the sequence of counts permits the use of vastly more efficient fast Fourier transform methods, we use this technique in this chapter. Alternate definitions of the PSD for point processes (and thus for the PG used to estimate them) exist; for example, a different PSD may be obtained from the real-valued discrete-time sequence of the interevent intervals. However, features in this PSD cannot be interpreted in terms of temporal frequency [40].

Figure 14.2 displays the PG for the visual system LGN data calculated using the count-based approach. (Throughout the text of this chapter we employ radian frequency ω [radians per unit time] to simplify the analysis, while figures are plotted in common frequency $f = \omega/2\pi$ [cycles per unit time] in accordance with common usage.) For low frequencies, the PG decays as $1/\omega^{\alpha}$, as expected for a fractal point process. Fitting a straight line (shown as dotted) to the doubly logarithmic plot of the PG, over the range from 0.002 Hz to 1 Hz, provides an estimate $\alpha \approx 0.67$. Similar results obtain for the other LGN and retinal ganglion cells (RGC) data sets that we have examined [36].

14.2.3 Fano Factor

Another useful measure of correlation over different timescales is provided by the Fano factor (FF), which is the variance of the number of events in a specified counting time T divided by the mean number of events in that counting time. In terms of the sequence of counts illustrated in Figure 14.1(c), the Fano factor is simply the variance of $\{Z_k\}$ divided by the mean of $\{Z_k\}$, i.e.,

$$F(T) \equiv \frac{\mathrm{E}[Z_k^2] - \mathrm{E}^2[Z_k]}{\mathrm{E}[Z_k]}. \tag{14.7}$$

The FF generally varies as a function of counting time T. The exception is the homogeneous Poisson point process (HPP), which is important as a benchmark in point process theory, just as the Gaussian is in the theory of continuous stochastic processes. For an HPP, the variance-to-mean ratio is always unity for any counting time T. Any deviation from unity in the

M. C. Teich, C. Heneghan, S. B. Lowen, and R. G. Turcott, in Wavelets in Medicine and Biology, edited by A. Aldroubi and M. Unser (CRC Press, Boca Raton, 1996), ch. 14, pp. 383-412.

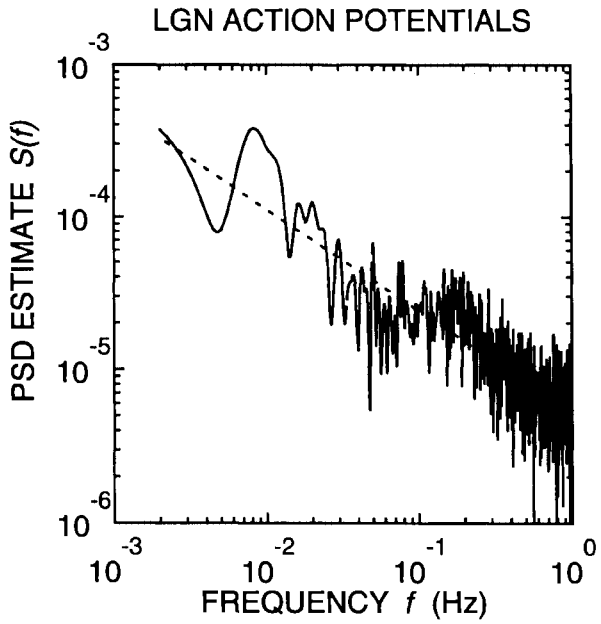

Figure 14.2
Doubly logarithmic plot of the count-based periodogram vs. frequency for the point process representing a nerve spike train recorded at the output of a visual-system relay neuron in the lateral geniculate nucleus (LGN) of the cat (solid curve). No external stimulus was present. The data segment analyzed here consists of 24,285 events with an average interevent time of 0.132 s, comprising a total duration of 3225 s. Over long timescales (low frequencies), the curve can be fit by a straight line (dotted) of slope -0.67, representing fractal behavior. This linear best fit to the data was calculated over the region from 0.002 Hz to 1 Hz.

value of $F(T)$ therefore indicates that the point process in question is not Poisson in nature. An excess above unity reveals that a sequence is "less ordered" than an HPP, while values below unity signify sequences which are "more ordered". For an FSPP, the FF can be shown to vary as $\sim T^{\alpha}$ for long counting times provided $0 < \alpha < 1$; therefore a straight-line fit to an estimate of $F(T)$ vs. T on a doubly logarithmic plot can also be used to estimate the fractal exponent.

Figure 14.3 shows the estimated FF curve for the same data set as shown in Figure 14.2. For counting times T greater than approximately 0.5 s, this curve behaves essentially as $\sim T^{\alpha}$. The estimated value is $\alpha = 0.65$ (dotted line), closely agreeing with the value obtained from the PG. Similar estimated FF curves emerge not only for other LGN data sets, but also from spike trains recorded from retinal ganglion cells [36].

M. C. Teich, C. Heneghan, S. B. Lowen, and R. G. Turcott, in Wavelets in Medicine and Biology, edited by A. Aldroubi and M. Unser (CRC Press, Boca Raton, 1996), ch. 14, pp. 383-412.

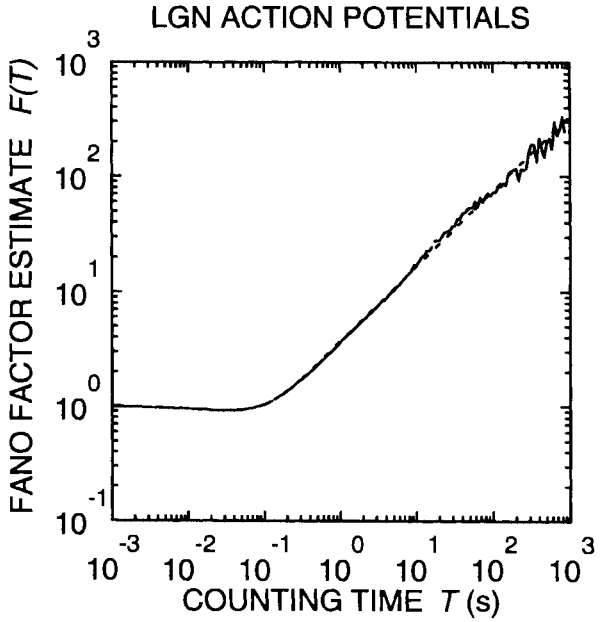

Figure 14.3
Doubly logarithmic plot of the Fano factor estimate vs. counting time, for the same spike train as used for Figure 14.2 (solid curve). Over long timescales, the curve can be fit by a straight line (dotted) of slope 0.65, representing fractal behavior with a similar exponent to that obtained from the PSD. This linear best fit to the data was calculated over the region from 0.3 s to 1000 s.

14.2.4 Allan Factor

The Allan variance, as opposed to the ordinary variance, is defined in terms of the variability of *successive* counts [3, 4]. In analogy with the Fano factor (FF), we define the Allan factor (AF) for the sequence of counts shown in Fig. 14.1 as

$$A(T) \equiv \frac{\mathrm{E}\left[(Z_{k+1} - Z_k)^2\right]}{2\mathrm{E}[Z_k]}. \tag{14.8}$$

As for the FF, the value of the Allan factor for the HPP is unity. For an FSPP, the AF also varies as $\sim T^{\alpha}$ for long counting times with $0 < \alpha < 3$; therefore a straight line fit of an estimate of $A(T)$ vs. T on a doubly logarithmic plot yields yet another estimate of the fractal exponent.

Figure 14.4 shows the estimated Allan factor curve for the same data set as shown in Figures 14.2 and 14.3. This measure appears to be considerably "rougher" than the FF, which is typical of the data sets we have analyzed.

M. C. Teich, C. Heneghan, S. B. Lowen, and R. G. Turcott, in Wavelets in Medicine and Biology, edited by A. Aldroubi and M. Unser (CRC Press, Boca Raton, 1996), ch. 14, pp. 383-412.

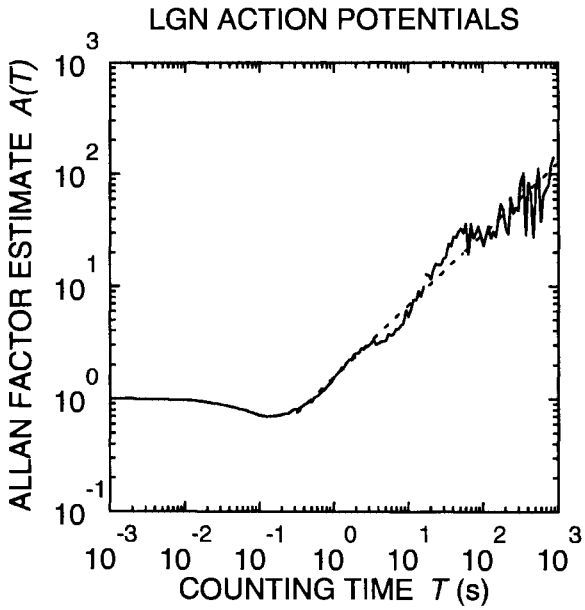

Figure 14.4
Doubly logarithmic plot of the Allan factor estimate vs. counting time, for the same spike train as used for Figures 14.2 and 14.3 (solid curve). Over long timescales, the curve can be fit by a straight line (dotted) of slope 0.64, representing fractal behavior with a similar exponent to that obtained from the PSD and the FF. This linear best fit to the data was calculated over the region from 0.3 s to 1000 s.

Nevertheless it is clear that for counting times T greater than approximately 0.5 s, its behavior can also be approximated as $\sim T^{\alpha}$. To estimate the value of α, a straight line fit to the doubly logarithmic plot of the estimate of $A(T)$ vs. counting time T was provided. The value of $\alpha = 0.64$ obtained agrees well with the values calculated using the PSD and FF. AF curves for other LGN and RGC data sets we have examined appear similar to this one.

14.2.5 Haar-Basis Representation of the Fano and Allan Factors

The Fano and Allan factors can be expressed as special cases of more general measures based on the statistics of the wavelet- and scaling-coefficient sequences of stochastic point processes. In this section, we outline the relation between the FF and AF on the one hand, and the wavelet- and scaling-coefficient-based measures on the other. In particular, we show that these measures coincide for the special case of the Haar wavelet basis.

M. C. Teich, C. Heneghan, S. B. Lowen, and R. G. Turcott, in Wavelets in Medicine and Biology, edited by A. Aldroubi and M. Unser (CRC Press, Boca Raton, 1996), ch. 14, pp. 383-412.

Scaling and Wavelet Coefficients for a Point Process

We first define the scaling and wavelet coefficients for the point process $dN(t)$. In analogy with the continuous-time definitions of these coefficients provided in Chapter 1, we define the scaling and wavelet coefficients of the point process as

$$(S_\varphi N)(a,k) = c[a,k] \equiv a^{-1/2} \int_{-\infty}^{+\infty} \overline{\varphi(u/a - k)}\, dN(u), \tag{14.9}$$

and

$$(W_\psi N)(a,k) = d[a,k] \equiv a^{-1/2} \int_{-\infty}^{+\infty} \overline{\psi(u/a - k)}\, dN(u), \tag{14.10}$$

where $\varphi(t)$ and $\psi(t)$ are the scaling and wavelet functions, respectively, and a is a real-valued scale factor by which the scaling and wavelet functions are dilated. The quantities $c[a,k]$ and $d[a,k]$ are notational conveniences for $(S_\varphi N)(a,k)$ and $(W_\psi N)(a,k)$, respectively. The overbar denotes complex conjugation.

The Haar Basis

The Haar basis plays a central role in uniting the Fano and Allan factors with their corresponding wavelet-based measures. As shown in Chapter 1, the scaling function for the Haar basis is defined as

$$\varphi_H(t) = \begin{cases} 1 & \text{for } 0 \le t < 1 \\ 0 & \text{otherwise} \end{cases} \tag{14.11}$$

while the wavelet function is defined as

$$\psi_H(t) = \begin{cases} 1 & \text{for } 0 \le t < 1/2 \\ -1 & \text{for } 1/2 \le t < 1 \\ 0 & \text{otherwise.} \end{cases} \tag{14.12}$$

Figures 14.5(a) and (b) display these functions.

Haar-Basis Scaling and Wavelet Coefficients

For the special case of the Haar wavelet basis introduced above, the integrals in Equations 14.9 and 14.10 are easily evaluated in terms of the counting process $N(t)$ as

$$c[a,k;\text{Haar}] = a^{-1/2}\{N(ka+a) - N(ka)\} \tag{14.13}$$

M. C. Teich, C. Heneghan, S. B. Lowen, and R. G. Turcott, in Wavelets in Medicine and Biology, edited by A. Aldroubi and M. Unser (CRC Press, Boca Raton, 1996), ch. 14, pp. 383-412.

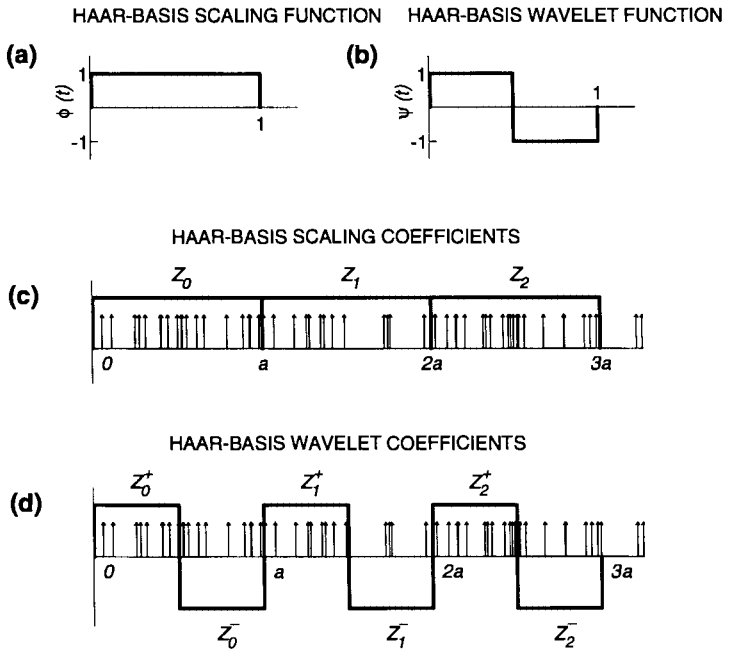

Figure 14.5
Determining the scaling and wavelet coefficients of a point process using the Haar basis. (a) The scaling function for the Haar basis, defined over the domain $[0,1]$. (b) The wavelet function for the Haar basis, defined over the domain $[0,1]$. (c) Using sequences of counts to evaluate the scaling coefficients for a point process $dN(t)$. In keeping with the notation of Figure 14.1(c), Z_k denotes the number of events, starting at time ka, and contained within a Haar wavelet that has been scaled by a. The scaling coefficient $c[a,k;\text{Haar}]$ is equal to $a^{-1/2}Z_k$. (d) Using sequences of counts to evaluate the wavelet coefficients for the same point process. The quantity Z_k^+ denotes the number of events, starting at time ka, during the positive portion of a Haar wavelet function (scaled by a); Z_k^- denotes the number of events during the negative half of the same Haar wavelet function. The wavelet coefficient $d[a,k;\text{Haar}]$ is equal to $a^{-1/2}(Z_k^+ - Z_k^-)$.

M. C. Teich, C. Heneghan, S. B. Lowen, and R. G. Turcott, in Wavelets in Medicine and Biology, edited by A. Aldroubi and M. Unser (CRC Press, Boca Raton, 1996), ch. 14, pp. 383-412.

and

$$d[a,k;\text{Haar}] = a^{-1/2}\{[N(ka+a/2)-N(ka)] - [N(ka+a)-N(ka+a/2)]\}, \tag{14.14}$$

where the notation $c[a,k;\text{Haar}]$ and $d[a,k;\text{Haar}]$ explicitly indicates that these scaling and wavelet coefficients are obtained using the Haar basis.

Figures 14.5(c) and (d) show graphically how the Haar-basis scaling and wavelet coefficients are calculated by windowing the original data set. The quantities Z_k, Z_k^+, and Z_k^- represent numbers of events contained beneath (or above) their associated rectangular windows. The unitless scale factor a is numerically equal to the duration of the counting window in seconds (which was the T used in the original definition of the FF and AF). The Haar-basis scaling and wavelet coefficients are therefore readily written in terms of the quantities

$$c[a,k;\text{Haar}] = a^{-1/2}Z_k \tag{14.15}$$

and

$$d[a,k;\text{Haar}] = a^{-1/2}\left(Z_k^+ - Z_k^-\right). \tag{14.16}$$

The connection proceeds by observing that the FF for a scale factor a (or a counting time T) is equal to the variance-to-mean ratio (FF) for counting windows of that duration. Considering the definition of the FF (Equation 14.7) in the context of Figures 14.5(c) and (d), we have

$$F(a) = \frac{\mathrm{E}\left[Z_k^2\right] - \mathrm{E}^2\left[Z_k\right]}{\mathrm{E}\left[Z_k\right]}. \tag{14.17}$$

Since $c[a,k;\text{Haar}] = a^{-1/2}Z_k$, the FF may be represented purely in terms of the Haar-basis scaling coefficients:

$$F(a) = a^{1/2}\left(\frac{\mathrm{E}\left\{c^2[a,k;\text{Haar}]\right\} - \mathrm{E}^2\left\{c[a,k;\text{Haar}]\right\}}{\mathrm{E}\left\{c[a,k;\text{Haar}]\right\}}\right). \tag{14.18}$$

Similarly, the AF can be expressed in terms of Z_k, Z_k^+, and Z_k^- as

$$A(a/2) = \frac{\mathrm{E}\left[\left(Z_k^+ - Z_k^-\right)^2\right]}{2\mathrm{E}\left[Z_k^+\right]}, \tag{14.19}$$

M. C. Teich, C. Heneghan, S. B. Lowen, and R. G. Turcott, in Wavelets in Medicine and Biology, edited by A. Aldroubi and M. Unser (CRC Press, Boca Raton, 1996), ch. 14, pp. 383-412.

which can be rewritten in terms of the scaling and wavelet coefficients as

$$A(a/2) = a^{1/2} \left(\frac{\mathrm{E}\left\{d^2[a,k;\mathrm{Haar}]\right\}}{\mathrm{E}\left\{c[a,k;\mathrm{Haar}]\right\}} \right). \tag{14.20}$$

The argument $a/2$ for $A(\cdot)$ reflects the fact that the counting windows in Figure 14.5(d) are half the length of the counting windows in Figure 14.5(c).

Equations 14.18 and 14.20 therefore demonstrate that, for the special case of the Haar basis, the scaling and wavelet coefficients of a point process provide a means of estimating the fractal exponent of an FSPP.

14.2.6 Wavelet-Based Fano and Allan Factors

Aside from the Haar basis, other wavelet bases may be employed for estimating α. The results are the wavelet Fano factor (WFF) and wavelet Allan factor (WAF), which are generalizations of the Fano and Allan factors respectively:

$$F_W(a) \equiv a^{1/2} \left(\frac{\mathrm{E}\left\{|c[a,k]|^2\right\} - \mathrm{E}^2\left\{|c[a,k]|\right\}}{\mathrm{E}\left\{|c[a,k]|\right\}} \right) \tag{14.21}$$

$$A_W(a) \equiv a^{1/2} \left(\frac{\mathrm{E}\left\{|d[a,k]|^2\right\}}{\mathrm{E}\left\{|c[a,k]|\right\}} \right), \tag{14.22}$$

where, by using the absolute value of the scaling and wavelet coefficients, we permit the use of complex-valued scaling and wavelet functions. Equation 14.22, defined here as the wavelet Allan factor (WAF), was first proposed as a measure by Flandrin and Abry [1, 2, 13, 14], who called it the wavelet Fano factor. More recently, they also considered a measure similar to $F_W(a)$ [1]. We have defined $A_W(a)$ to coincide with $A(a/2)$ for the special case of the Haar basis, to avoid a superfluous factor of 2 in the definition of the WAF.

These measures permit the estimation of the fractal exponent of an FSPP. To demonstrate this, we first calculate the expected values of $|c[a,k]|$, $|c[a,k]|^2$, and $|d[a,k]|^2$, employing the coincidence rate $G(\tau)$ of a fractal point process defined in Equation 14.5, and the scaling and wavelet functions $\varphi(t)$ and $\psi(t)$, respectively. The expected value of $|c[a,k]|$ is

$$\mathrm{E}\left\{|c[a,k]|\right\} = a^{-1/2} \left| \int_{-\infty}^{+\infty} \overline{\varphi(t/a - k)}\, \mathrm{E}[dN(t)] \right| \tag{14.23}$$

M. C. Teich, C. Heneghan, S. B. Lowen, and R. G. Turcott, in Wavelets in Medicine and Biology, edited by A. Aldroubi and M. Unser (CRC Press, Boca Raton, 1996), ch. 14, pp. 383-412.

$$= a^{-1/2} \left| \int_{-\infty}^{+\infty} \overline{\varphi(t/a - k)}\, \lambda\, dt \right|$$

$$= \lambda a^{1/2} \left| \int_{-\infty}^{+\infty} \overline{\varphi(z)}\, dz \right|$$

$$= \lambda a^{1/2},$$

since $\mathrm{E}[dN(t)] = \lambda\, dt$ by definition, with λ the mean rate of the point process. Note that we have chosen the scaling function to be normalized to unit area.

The expected value of $|c[a,k]|^2$ is readily calculated as

$$\mathrm{E}\left\{|c[a,k]|^2\right\} \tag{14.24}$$

$$= a^{-1} \int_{-\infty}^{+\infty} \int_{-\infty}^{+\infty} \varphi(t/a - k)\overline{\varphi(u/a - k)}\, \mathrm{E}[dN(t)\, dN(u)]$$

$$= a^{-1} \int_{-\infty}^{+\infty} \int_{-\infty}^{+\infty} \varphi(t/a - k)\overline{\varphi(u/a - k)}\, G(t - u)\, dt\, du,$$

where $G(t)$ is the coincidence rate for the process. By using the substitutions $y \equiv u/a - b$ and $z \equiv (t - u)/a$, for a stationary point process we obtain

$$\mathrm{E}\left\{|c[a,k]|^2\right\} = a \int_{-\infty}^{+\infty} (S_\varphi \varphi)(1,z) G(za)\, dz, \tag{14.25}$$

where

$$(S_\varphi \varphi)(1,z) \equiv \int_{-\infty}^{+\infty} \varphi(y)\overline{\varphi(y - z)}\, dy \tag{14.26}$$

is the continuous scaling transform of the scaling function itself, at unit scale. Similarly, the expected value of $|d[a,k]|^2$ can be calculated as

$$\mathrm{E}\left\{|d[a,k]|^2\right\} = a \int_{-\infty}^{+\infty} (W_\psi \psi)(1,z) G(za)\, dz, \tag{14.27}$$

with

$$(W_\psi \psi)(1,z) = \int_{-\infty}^{+\infty} \psi(y)\overline{\psi(y - z)}\, dy \tag{14.28}$$

the continuous wavelet transform of the wavelet function $\psi(t)$.

M. C. Teich, C. Heneghan, S. B. Lowen, and R. G. Turcott, in Wavelets in Medicine and Biology, edited by A. Aldroubi and M. Unser (CRC Press, Boca Raton, 1996), ch. 14, pp. 383-412.

For an ideal FSPP, the CR assumes the form given in Equation 14.5; substituting this into Equation 14.25 yields for the scaling coefficients

$$\begin{aligned}
\mathrm{E}\left\{|c[a,k]|^2\right\} &= a\int_{-\infty}^{+\infty}(S_\varphi\varphi)(1,z)\lambda\delta(az)\,dz \qquad (14.29)\\
&\quad +\lambda^2 a\int_{-\infty}^{+\infty}(S_\varphi\varphi)(1,z)\,dz\\
&\quad +\lambda^2 a\int_{-\infty}^{+\infty}(S_\varphi\varphi)(1,z)(a/\tau_0)^{\alpha-1}|z|^{\alpha-1}\,dz\\
&= a(\lambda/a)(S_\varphi\varphi)(1,0)+\lambda^2 a\\
&\quad +\lambda^2 a^\alpha\tau_0^{1-\alpha}\int_{-\infty}^{+\infty}(S_\varphi\varphi)(1,z)|z|^{\alpha-1}\,dz\\
&= \lambda+\lambda^2 a+\lambda^2 a^\alpha\tau_0^{1-\alpha}\int_{-\infty}^{+\infty}(S_\varphi\varphi)(1,z)|z|^{\alpha-1}\,dz,
\end{aligned}$$

where we have used the identity $\int_{-\infty}^{+\infty}(S_\varphi\varphi)(1,z)\,dz = 1$ appropriate for a scaling function of unit area, and we have also normalized the scaling function to have unit energy, so that $(S_\varphi\varphi)(1,0) = 1$. (The scaling function $\varphi(t)$ may be defined to have both unity area and unity energy. For unnormalized scaling functions, the results are qualitatively the same, although notationally more cumbersome.)

In a similar manner, the expected value of the absolute square of the wavelet coefficients for the fractal point process is calculated to be

$$\begin{aligned}
\mathrm{E}\left\{|d[a,k]|^2\right\} &= a\int_{-\infty}^{+\infty}(W_\psi\psi)(1,z)\lambda\delta(az)\,dz \qquad (14.30)\\
&\quad +\lambda^2 a\int_{-\infty}^{+\infty}(W_\psi\psi)(1,z)\,dz\\
&\quad +\lambda^2 a\int_{-\infty}^{+\infty}(W_\psi\psi)(1,z)(a/\tau_0)^{\alpha-1}|z|^{\alpha-1}\,dz\\
&= a(\lambda/a)(W_\psi\psi)(1,0)+\lambda^2 a\cdot 0
\end{aligned}$$

M. C. Teich, C. Heneghan, S. B. Lowen, and R. G. Turcott, in Wavelets in Medicine and Biology, edited by A. Aldroubi and M. Unser (CRC Press, Boca Raton, 1996), ch. 14, pp. 383-412.

$$+\lambda^2 a^\alpha \tau_0^{1-\alpha} \int_{-\infty}^{+\infty} (W_\psi \psi)(1,z)|z|^{\alpha-1}\, dz$$

$$= \lambda + \lambda^2 a^\alpha \tau_0^{1-\alpha} \int_{-\infty}^{+\infty} (W_\psi \psi)(1,z)|z|^{\alpha-1}\, dz,$$

where this time we invoke the identities $\int_{-\infty}^{+\infty}(W_\psi\psi)(1,z)\,dz = 0$ for any admissible wavelet, and $(W_\psi\psi)(1,0) = 1$, since the scaling and wavelet functions have equal energy.

Using Equations 14.23 and 14.29 for a FSPP, the WFF defined in Equation 14.21 becomes

$$F_W(a) = a^{1/2}\left(\frac{\lambda + \lambda^2 a + \lambda^2 a^\alpha \tau_0^{1-\alpha} \int_{-\infty}^{+\infty}(S_\varphi\varphi)(1,z)|z|^{\alpha-1}\,dz - \lambda^2 a}{\lambda a^{1/2}}\right)$$

$$= 1 + \frac{\alpha(\alpha+1)}{2}\left(\frac{a}{a_0}\right)^\alpha \int_{-\infty}^{+\infty}(S_\varphi\varphi)(1,z)|z|^{\alpha-1}\,dz, \qquad (14.31)$$

where we implicitly define a_0 by the relation

$$2\lambda a_0^\alpha = \alpha(\alpha-1)\tau_0^{\alpha-1} \qquad (14.32)$$

for notational convenience [22]. The integral in Equation 14.31 depends on the scaling function φ and on the fractal exponent α, but not on the scale a; thus it does not affect the overall power-law behavior of $F_W(a)$. For large values of a, the wavelet Fano factor increases essentially as $\sim a^\alpha$. Accordingly, the fractal exponent can be readily estimated from the slope of the straight-line region on a doubly logarithmic plot of an estimate of $F_W(a)$ vs. scale a.

Similarly, the wavelet Allan factor for a fractal point process follows the form

$$A_W(a) = 1 + \frac{\alpha(\alpha+1)}{2}\left(\frac{a}{a_0}\right)^\alpha \int_{-\infty}^{+\infty}(W_\psi\psi)(1,z)|z|^{\alpha-1}\,dz, \qquad (14.33)$$

with the integral in Equation 14.33 also independent of a, so that the fractal exponent α may also be estimated from the slope of the straight-line region on a doubly logarithmic plot of an estimate of $A_W(a)$ vs. scale a.

The integrals given in Equations 14.9 and 14.10 for the scaling and wavelet coefficients can be numerically approximated for a point process by

M. C. Teich, C. Heneghan, S. B. Lowen, and R. G. Turcott, in Wavelets in Medicine and Biology, edited by A. Aldroubi and M. Unser (CRC Press, Boca Raton, 1996), ch. 14, pp. 383-412.

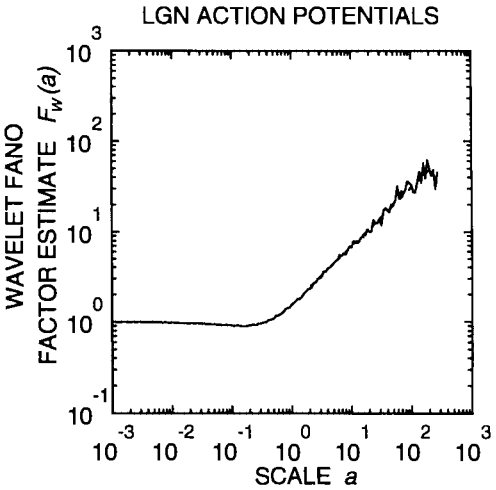

Figure 14.6
Doubly logarithmic plot of the wavelet Fano factor estimate vs. scale a, for the same spike train as used for Figures 14.2, 14.3, and 14.4 (solid curve). The Daubechies four-tap scaling and wavelet functions were used to calculate the estimated WFF. The prototype wavelet function was taken to be of duration 1 s for scale $a = 1$. Over long timescales, the curve can be fit by a straight line (dotted) of slope 0.65, representing fractal behavior with a similar exponent to that obtained from the PSD, FF, and AF. This linear best fit to the data was calculated over the region from 1 to 250.

using a summation in conjunction with well-sampled versions of the scaling and wavelet functions. Figure 14.6 shows the estimates of the wavelet Fano factor calculated in this manner for the same data set as shown in Figures 14.2, 14.3, and 14.4 (Daubechies four-tap scaling and wavelet functions [9] were used in this implementation). The prototype wavelet was set to have a duration of 1 second at scale $a = 1$. For scales a greater than approximately 1, the estimate of the WFF behaves essentially as $\sim a^{\alpha}$. To estimate the value of α, a straight-line fit to the doubly logarithmic plot of this estimated $F_W(a)$ vs. a was provided. The resulting value is $\alpha = 0.65$ (dotted line), closely agreeing with the value obtained from the PSD, FF, and AF.

Figure 14.7 shows the estimate of the wavelet Allan factor calculated for the same data set as shown in Figures 14.2–14.6. For scales a greater than approximately 5, this estimate behaves essentially as $\sim a^{\alpha}$, though like the estimated Allan factor shown in Figure 14.4, it is rough in appearance. As before, to estimate the value of α, a straight-line fit to the doubly logarithmic plot of the estimated $F_W(a)$ vs. a was provided, resulting in a value of $\alpha = 0.62$ (dotted line). Thus all five methods for estimating the

M. C. Teich, C. Heneghan, S. B. Lowen, and R. G. Turcott, in Wavelets in Medicine and Biology, edited by A. Aldroubi and M. Unser (CRC Press, Boca Raton, 1996), ch. 14, pp. 383-412.

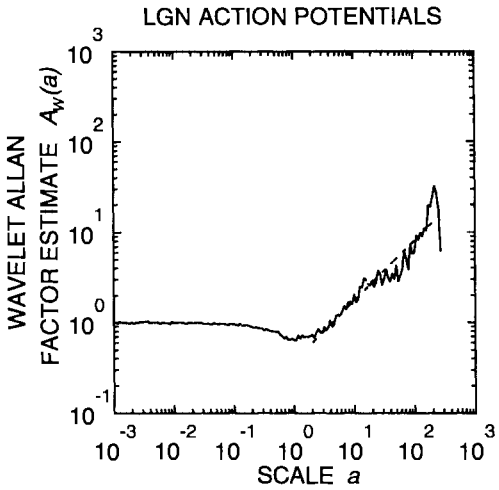

Figure 14.7
Doubly logarithmic plot of the wavelet Allan factor estimate vs. time, for the same spike train as used for Figures 14.2, 14.3, 14.4, and 14.6. The same wavelet basis was used as in Figure 14.6. Over long timescales, the curve can be fit by a straight line (dotted) of slope 0.62, representing fractal behavior with a similar exponent to that of the PSD, FF, AF, and WFF. This linear best fit to the data was calculated over the region from 1 to 250.

fractal exponent, the PSD, FF, AF, WFF, and WAF, yield values in close agreement.

14.3 Comparison of the Estimation Properties of Existing Techniques and Wavelet-Based Techniques

The question naturally arises: does this agreement extend to arbitrary data sets, and if not, which technique provides the most reliable estimate of the fractal exponent α?

To address this issue we undertook a systematic examination of the bias and variance of each of these estimators. We simulated 50 runs of an SFRP at each of three different input values of α: $\alpha = 0.2$, 0.5, and 0.8. Each simulation was chosen to be 10^5 seconds long with an expected interevent time of 1.0 s. The PSD, FF, AF, WFF, and WAF were estimated for each of the 150 simulations, and the fractal exponents were in turn estimated from these statistics by using straight-line fits over a fixed region of each of the 750 individual doubly logarithmic curves. The means and standard

M. C. Teich, C. Heneghan, S. B. Lowen, and R. G. Turcott, in Wavelets in Medicine and Biology, edited by A. Aldroubi and M. Unser (CRC Press, Boca Raton, 1996), ch. 14, pp. 383-412.

Table 14.1
Performance summary of the five fractal-exponent estimators described in Section 14.2 (PSD, FF, AF, WFF, and WAF) when applied to 50 independent realizations of an SFRP for each of three values of the fractal exponent α (0.2, 0.5, and 0.8).

	Theoretical Fractal Exponent		
	0.2	0.5	0.8
PSD	0.332 ± 0.014	0.480 ± 0.017	0.603 ± 0.012
FF	0.313 ± 0.065	0.425 ± 0.081	0.591 ± 0.075
AF	0.337 ± 0.034	0.482 ± 0.055	0.645 ± 0.041
WFF	0.322 ± 0.068	0.424 ± 0.084	0.607 ± 0.069
WAF	0.332 ± 0.025	0.482 ± 0.034	0.614 ± 0.034

Note: For each measure, the mean value $\pm$ the standard deviation is presented. The estimates were obtained over the following frequency and time ranges: PSD: 0.001–0.1 Hz; FF and AF: 5–1000 s; WFF and WAF: 25–2500. For the WFF and the WAF, the range refers to the value of the scale factor a used to dilate the mother scaling and wavelet functions.

deviations of these fractal exponent estimates are listed in Table 14.1 and presented graphically in Figure 14.8(a). The ranges over which the estimates were obtained are indicated in the table caption.

Figure 14.8(a) reveals at a glance that all of the measures perform quite poorly for $\alpha = 0.2$ and $\alpha = 0.8$. The observed bias towards the value 0.5 also emerges when estimating the fractal exponent of a superposition of SFRPs (Figure 8 of [22]). This bias is not fully understood; part undoubtedly stems from the necessity for finite data-length simulations, and part arises from the need for imposing cutoffs in the simulation of the SFRP (A and B in Equation 14.3). In fact, the simulation process itself may be inherently biased. The simulations shown here follow the techniques used in [22], where the IIPDF was chosen to have a power-law decay with an exponent of $\alpha - 3$; this yielded physiologically plausible simulations of neural spike trains. Changing this exponent to $-(\alpha + 1)$ somewhat reduced the bias in the estimate of α, but the resulting simulations no longer resembled neuronal behavior. However, this reduction in the bias does support the claim that the bias may in large part stem from simulation effects.

Therefore we focus instead on the relative differences between fractal exponent estimates obtained through wavelet-based measures and those obtained from the PSD, FF, and AF, and in particular on the means and standard deviations provided in Table 14.1 and Figure 14.8(a). The means do not show a significant difference; employing the PSD, AF, and WAF yields estimated mean values of α within 0.04 of each other, with the values corresponding to the FF and WFF only slightly farther apart. However,

M. C. Teich, C. Heneghan, S. B. Lowen, and R. G. Turcott, in Wavelets in Medicine and Biology, edited by A. Aldroubi and M. Unser (CRC Press, Boca Raton, 1996), ch. 14, pp. 383-412.

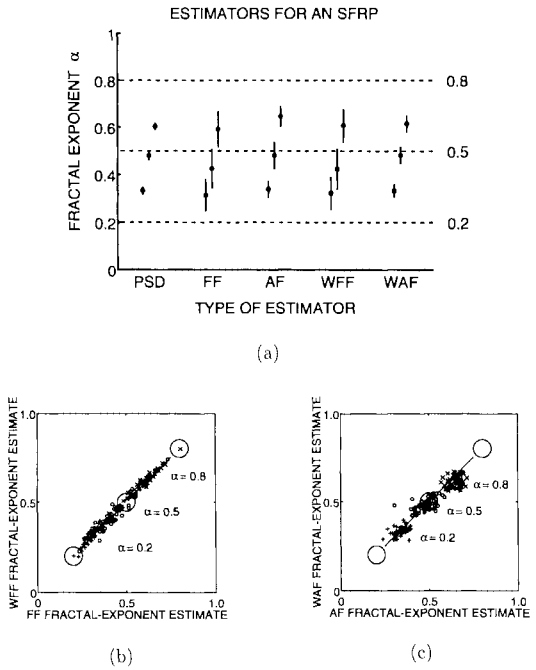

Figure 14.8

Performance summary of the five estimators considered in this chapter (PSD, FF, AF, WFF, and WAF). (a) Graphical representation of the data presented in Table 14.1. The mean values of 50 estimates for the fractal exponent of the SFRP, for each of the three different values of α, are marked by dots. The ± 1-SD regions are indicated by the vertical lines projecting from each dot. All of the estimates show strong bias for $\alpha = 0.2$ and $\alpha = 0.8$; only the measures employing the FF and WFF are significantly biased for $\alpha = 0.5$. From the perspective of the variance of the estimator, the PSD-based method is best (least variance), with the AF and WAF achieving nearly as low a variance, and the FF and WFF exhibiting the worst performance. (b) Relation between the WFF- and the FF-based estimates. The estimated value of α using the WFF is plotted against the estimated value from the FF; the correlation coefficient is 0.99. This consistency is gratifying, since the two measures are essentially the same, differing only in the change of wavelet basis from the Daubechies four-tap (for the WFF) to the Haar basis (for the FF). Both estimators show strong bias for $\alpha = 0.2$ and $\alpha = 0.8$, and have a high variance (see Table 14.1 for numerical values). (c) Relation between the WAF- and the AF-based estimates. The estimated value of α using the WAF is plotted against the estimated value from the AF; these are highly correlated, for the same reason as in (b), with a correlation coefficient of 0.95. Both estimators show strong bias for $\alpha = 0.2$ and $\alpha = 0.8$, but have a moderately low variance (see Table 14.1 for numerical values).

M. C. Teich, C. Heneghan, S. B. Lowen, and R. G. Turcott, in Wavelets in Medicine and Biology, edited by A. Aldroubi and M. Unser (CRC Press, Boca Raton, 1996), ch. 14, pp. 383-412.

Figure 14.8(a) clearly shows that the standard deviations using the FF and WFF methods are significantly greater than those for the other measures, and this will be further explored in Section 14.4.

We now turn to the correlation between the estimates provided by the FF/WFF and AF/WAF pairs. A positive correlation is to be anticipated, since we have shown theoretically how the WFF and WAF are generalizations of the FF and AF, respectively. Figure 14.8(b) shows a scatter plot of the 150 estimates of α obtained from the FF and the WFF. The centers of the three large circles correspond to zero error in estimating the fractal exponent for the three values of α used to simulate the process, and the lines connecting the circles indicates where the two estimates coincide. Since the estimate pairs are strongly clustered along these lines, they are strongly correlated, confirming that the WFF is indeed closely related to the FF; the correlation coefficient is 0.99. Figure 14.8(c) shows a similar scatter plot obtained from the AF and the WAF. Again the estimate pairs are strongly clustered along the 45° line, indicating that they are strongly correlated, and that the WAF is closely related to the AF. For this pair the correlation coefficient assumes a value of 0.95. Though the estimates of the WFF and WAF displayed in Figure 14.8 are specifically calculated using a Daubechies four-tap wavelet basis, we have determined that the results do not vary significantly for different wavelet bases [15]; there tends to be a slight increase in the variance of the estimators as the number of vanishing moments of the wavelet increases—see Section 14.4.

14.4 Discussion

An interesting feature that emerges from the SFRP simulations summarized in Figure 14.8 is the consistently lower variances in fractal-exponent estimation exhibited when using AF- and WAF-based methods in comparison with those of the FF and WFF. Flandrin and Abry [1, 2, 12–14] suggested that this might relate to the behavior of the Fourier transforms of the scaling and wavelet functions. To investigate this supposition, we recast Equations 14.25 and 14.27 from time-domain integrals into frequency-domain ones. Thus, Equation 14.25 becomes

$$\mathrm{E}\left\{|c[a,k]|^2\right\} = a\int_{-\infty}^{+\infty}(S_\varphi\varphi)(1,z)G(za)\,dz \tag{14.34}$$

$$= \int_{-\infty}^{+\infty}(S_\varphi\varphi)(1,z/a)G(z)\,dz$$

M. C. Teich, C. Heneghan, S. B. Lowen, and R. G. Turcott, in Wavelets in Medicine and Biology, edited by A. Aldroubi and M. Unser (CRC Press, Boca Raton, 1996), ch. 14, pp. 383-412.

$$= \int_{-\infty}^{+\infty} \left[\int_{-\infty}^{+\infty} \varphi(y)\overline{\varphi(y - z/a)}dy \right] G(z)\, dz$$

$$= \frac{1}{2\pi} \int_{-\infty}^{+\infty} \int_{-\infty}^{+\infty} |\hat{\varphi}(\omega)|^2 \exp(i\omega z/a) G(z)\, d\omega\, dz$$

$$= \frac{1}{2\pi} \int_{-\infty}^{+\infty} |\hat{\varphi}(\omega)|^2 S(\omega/a)\, d\omega$$

$$= \frac{1}{2\pi} a \int_{-\infty}^{+\infty} |\hat{\varphi}(\omega a)|^2 S(\omega)\, d\omega,$$

where $\hat{\varphi}(\omega)$ is the Fourier transform of $\varphi(t)$, and

$$S(\omega) = \int_{-\infty}^{+\infty} G(z) \exp(-i\omega z)\, dz \tag{14.35}$$

is the PSD of the point process, as defined in Section 14.2.2. Similarly, Equation 14.27 may be expressed as

$$\mathrm{E}\left\{|d[a,k]^2|\right\} = \frac{1}{2\pi} \int_{-\infty}^{+\infty} \left|\hat{\psi}(\omega)\right|^2 S(\omega/a)\, d\omega \tag{14.36}$$

$$= \frac{a}{2\pi} \int_{-\infty}^{+\infty} \left|\hat{\psi}(\omega a)\right|^2 S(\omega)\, d\omega.$$

The forms of the integrals in Equations 14.34 and 14.36 provide some insight into the relative performances of the five fractal exponent estimators studied. For an FSPP, the PSD follows the form of Equation 14.6 and diverges at low frequencies. Any practical FSPP will have cutoff frequencies, however, beyond which the fractal scaling no longer holds, and the PSD will therefore assume some finite value at low frequencies. Fractal processes naturally exhibit fluctuations on all frequency scales, with the lowest frequencies displaying the largest fluctuations, in proportion to the PSD. Therefore the low-frequency asymptote of a PSD estimate can fluctuate widely among different simulations of the same FSPP. By definition, $|\hat{\varphi}(0)| = 1$ and is continuous at $\omega = 0$, so that the integral in Equation 14.34 does not converge for a fractal point process with $0 < \alpha < 1$ and therefore explicitly depends on the low frequency asymptote. Thus $\mathrm{E}\left\{|c[a,k]|^2\right\}$ depends directly on this fluctuating quantity, and the estimate of the FF and

M. C. Teich, C. Heneghan, S. B. Lowen, and R. G. Turcott, in Wavelets in Medicine and Biology, edited by A. Aldroubi and M. Unser (CRC Press, Boca Raton, 1996), ch. 14, pp. 383-412.

WFF should exhibit the largest variance. Indeed, estimates of individual FF and WFF plots for the SFRP simulations used in this chapter exhibit wide fluctuations from run to run. Although each individual estimated FF or WFF curve appears smooth, overlays of these plots show a wide range of slopes for the same starting value of the fractal exponent α, therefore yielding wide variation in the estimates of α.

The Fourier transforms of wavelet functions, however, attain a value of zero for zero frequency, and are also continuous at this point. Therefore the behavior of the integrand in Equation 14.36 near the origin for an FSPP depends on both the divergence in the PSD and the tendency of $|\hat{\psi}(\omega)|$ to go to zero. The behavior of $|\hat{\psi}(\omega)|$ near the origin may be described by the number of vanishing moments R of the wavelet, defined as the largest integer R for which

$$\int_{-\infty}^{+\infty} t^R \psi(t)\, dt = 0.$$

For a wavelet $\psi(t)$ with R vanishing moments, the magnitude of its Fourier transform $|\hat{\psi}(\omega)|$ varies as $\sim \omega^{R+\epsilon}$ for $\omega \to 0$, where $0 < \epsilon \leq 1$. Therefore, the integral in Equation 14.36 converges without a low-frequency asymptote for any $\alpha < 1 + 2R$. The Haar basis has $R = 0$ exactly; for our simulations $\alpha < 1$, so $\mathrm{E}\left\{|d[a,k]|^2\right\}$ does not depend on the fluctuating low-frequency asymptote, and estimates of the AF should exhibit lower variance than those of the FF and WFF. In fact, for the Haar basis $|\hat{\psi}(\omega)|$ varies as $\sim \omega^1$ so that the Allan factor converges for $\alpha < 3$. For the Daubechies four-tap wavelet that we have used, $R = 2$, so that the cutoffs do not greatly affect the integral for $\alpha < 5$. We expect estimates of the WAF to exhibit similar variance to those of the AF, since in our simulations we employ fractal exponents in the range $0 < \alpha < 1$. The WAF should prove more useful than the AF for FSPPs with $\alpha > 3$. In contrast to the FF and the WFF, individual AF and WAF estimates exhibit somewhat smaller fluctuations from plot to plot. These Allan-based estimates appear somewhat more ragged than those of the FF and WAF, but slopes for these plots in fact show less variation, and yield estimates of α with somewhat less variance.

Finally, we expect the PG to have the lowest variance of all, since it depends on all frequencies and thus deemphasizes the effect of the low-frequency fluctuations. Simulations validate this reasoning. Individual PG plots indeed exhibit the widest variation of all, yet the estimates of the fractal exponent α exhibit the least variance of the five measures studied. For the values of α we have chosen, the wavelet-based measures exhibit similar performance to those of their Haar-basis counterparts. In short, the Allan-based methods outperform those based on Fano factors, and the PG yields the best performance of all.

M. C. Teich, C. Heneghan, S. B. Lowen, and R. G. Turcott, in Wavelets in Medicine and Biology, edited by A. Aldroubi and M. Unser (CRC Press, Boca Raton, 1996), ch. 14, pp. 383-412.

14.5 Conclusion

We have defined two wavelet-based measures for estimating the fractal exponent of a point process: the wavelet Fano factor and wavelet Allan factor. These arise as natural generalizations of two simple count-based measures: the Fano factor and Allan factor, respectively. We have shown that, at least for the standard fractal renewal process, the wavelet-based techniques reveal their Fano- and Allan-factor origins by exhibiting similar biases and variances. The AF and the WAF outperform the FF and the WFF for the SFRP, apparently because of the increased number of vanishing moments in the frequency domain of wavelet functions compared to scaling functions. Carrying this argument further, one might expect that the WAF would outperform the AF for wavelet bases with at least one vanishing moment. SFRP simulations reveal that this does not happen, however, indicating that the addition of further vanishing moments is offset by the effective widening of the support of the wavelet basis, leading to fewer independent values of wavelet and scaling coefficients for a given finite data set [15]. Still, the fractal-exponent estimation properties of the power spectral density, a Fourier-transform based method, appear to surpass the other methods investigated, at least for this simulation of the SFRP; other types of FSPPs, or even other variations of the SFRP, might well yield different results. Thus wavelet-based measures can be fruitfully added to our armament of techniques for estimating the fractal exponent of an FSPP.

14.6 Acknowledgments

This work was supported by the Office of Naval Research under grant N00014-92-J-1251, by the Joint Services Electronics Program through the Columbia Radiation Laboratory, and by the Whitaker Foundation under Grant No. CU01455801. The authors are grateful to Patrice Abry (École Normale Supérieure de Lyon), Patrick Flandrin (École Normale Supérieure de Lyon), and Cormac Herley (Hewlett-Packard Laboratories) for valuable discussions. E. Kaplan and T. Ozaki of Rockefeller University kindly provided us with the visual-system spike trains used as examples in this chapter.

M. C. Teich, C. Heneghan, S. B. Lowen, and R. G. Turcott, in Wavelets in Medicine and Biology, edited by A. Aldroubi and M. Unser (CRC Press, Boca Raton, 1996), ch. 14, pp. 383-412.

References

[1] P. Abry, Transformées en ondelettes: Analyses multirésolution et signaux de presion en turbulence, Doctoral thesis, Université Claude Bernard—Lyon I, France (1994).

[2] P. Abry and P. Flandrin, Wavelet-based Fano factor for long-range dependent point processes, *Proc. 16th Annu. Int. Conf. IEEE Eng. Med. Biol. Soc.* (Baltimore, MD, 1994), pp. 1330–1331.

[3] D. W. Allan, Statistics of atomic frequency standards, *Proc. IEEE* **54**, 221–230 (1966).

[4] J. A. Barnes and D. W. Allan, A statistical model of flicker noise, *Proc. IEEE* **54**, 176–178 (1966).

[5] R. J. Barton and H. V. Poor, Signal detection in fractional Gaussian noise, *IEEE Trans. Inform. Theory* **34**, 943–959 (1988).

[6] J. Beran, Statistical methods for data with long-range dependence, *Stat. Sci.* **7**, 404–427 (1992).

[7] J. M. Berger and B. B. Mandelbrot, A new model for the clustering of errors on telephone circuits, *IBM J. Res. Dev.* **7**, 224–236 (1963).

[8] D. R. Cox and V. Isham, *Point Processes* (Chapman and Hall, London, 1980).

[9] I. Daubechies, Orthonormal bases of compactly supported wavelets, *Commun. Pure Appl. Math.* **41**, 909–996 (1988).

[10] L. J. DeFelice and A. Isaac, Chaotic states in a random world: relationship between the nonlinear differential equations of excitability and the stochastic properties of ion channels, *J. Stat. Phys.* **70**, 339–354 (1993).

[11] P. Flandrin, On the spectrum of fractional Brownian motions, *IEEE Trans. Inf. Theory* **35**, 197–199 (1989).

[12] P. Flandrin, Wavelet analysis and synthesis of fractional Brownian motion, *IEEE Trans. Inf. Theory* **38**, 910–917 (1992).

[13] P. Flandrin, Time-scale analyses and self-similar stochastic processes, *Proc. NATO Adv. Study Inst. Wavelets and Their Applications* (Il Ciocco, Italy, 1992).

M. C. Teich, C. Heneghan, S. B. Lowen, and R. G. Turcott, in Wavelets in Medicine and Biology, edited by A. Aldroubi and M. Unser (CRC Press, Boca Raton, 1996), ch. 14, pp. 383-412.

[14] P. Flandrin and P. Abry, Tracking long-range dependencies with wavelets, *Proc. 1994 IEEE-IMS Workshop Inf. Stat.* (Alexandria, VA, 1994), p. 54.

[15] C. Heneghan, S. B. Lowen, and M. C. Teich, Wavelet analysis for estimating the fractal properties of neural firing patterns, *Proc. Computational Neurosci.*, 1995.

[16] A. H. Kumar and D. H. Johnson, Analyzing and modeling fractal intensity point processes, *J. Acoust. Soc. Am.* **93**, 3365–3373 (1993).

[17] L. S. Liebovitch and T. I. Tóth, Using fractals to understand the opening and closing of ion channels, *Ann. Biomed. Eng.* **18**, 177–194 (1990).

[18] S. B. Lowen and M. C. Teich, Fractal renewal processes as a model of charge transport in amorphous semiconductors, *Phys. Rev. B* **46**, 1816–1819 (1992).

[19] S. B. Lowen and M. C. Teich, Fractal renewal processes generate $1/f$ noise, *Phys. Rev. E* **47**, 992–1001 (1993).

[20] S. B. Lowen and M. C. Teich, Fractal renewal processes, *IEEE Trans. Inf. Theory* **39**, 1669–1671 (1993).

[21] S. B. Lowen and M. C. Teich, Fractal auditory-nerve firing patterns may derive from fractal switching in sensory hair-cell ion channels, in *Noise in Physical Systems and* $1/f$ *Fluctuations* (AIP Conference Proceedings **285**), eds. P. H. Handel and A. L. Chung (American Institute of Physics, New York, 1993), pp. 781–784.

[22] S. B. Lowen and M. C. Teich, Estimation and simulation of fractal stochastic point processes, *Fractals* **3**, 183–210 (1995).

[23] B. B. Mandelbrot, Self-similar error clusters in communication systems and the concept of conditional stationarity, *IEEE Trans. Commun. Tech.* **13**, 71–90 (1965).

[24] B. B. Mandelbrot, *The Fractal Geometry of Nature* (W. H. Freeman, New York, 1983).

[25] K. Matsuo, B. E. A. Saleh, and M. C. Teich, Cascaded Poisson processes, *J. Math. Phys.* **23**, 2353–2364 (1982).

[26] W. Rudin, *Principles of Mathematical Analysis*, 3rd ed. (McGraw Hill, New York, 1976), p. 197.

M. C. Teich, C. Heneghan, S. B. Lowen, and R. G. Turcott, in Wavelets in Medicine and Biology, edited by A. Aldroubi and M. Unser (CRC Press, Boca Raton, 1996), ch. 14, pp. 383-412.

[27] B. K. Ryu and S. B. Lowen, Modeling self-similar traffic with the fractal-shot-noise-driven Poisson process, Cent. for Telecomm. Res., Tech. Rep. 392-94-39 (Columbia University, New York, 1994).

[28] B. Sakmann and E. Neher, *Single-Channel Recording* (Plenum, New York, 1983).

[29] H. E. Schepers, J. H. G. M. van Beek, and J. B. Bassingthwaighte, Four methods to estimate the fractal dimension from self-affine signals, *IEEE Eng. Med. Biol. Mag.* **11**, 57–64 (1992).

[30] M. C. Teich, Fractal character of the auditory neural spike train, *IEEE Trans. Biomed. Eng.* **36**, 150–160 (1989).

[31] M. C. Teich, R. G. Turcott, and S. B. Lowen, The fractal doubly stochastic Poisson point process as a model for the cochlear neural spike train, in *The Mechanics and Biophysics of Hearing* (*Lecture Notes in Biomathematics, Vol. 87*), eds. P. Dallos, C. D. Geisler, J. W. Matthews, M. A. Ruggero, and C. R. Steele (Springer-Verlag, New York, 1990), pp. 354–361.

[32] M. C. Teich, D. H. Johnson, A. R. Kumar, and R. G. Turcott, Rate fluctuations and fractional power-law noise recorded from cells in the lower auditory pathway of the cat, *Hear. Res.* **46**, 41–52 (1990).

[33] M. C. Teich, Fractal neuronal firing patterns, in *Single Neuron Computation*, eds. T. McKenna, J. Davis, and S. Zornetzer (Academic, Boston, 1992), pp. 589–625.

[34] M. C. Teich and S. B. Lowen, Fractal patterns in auditory nerve-spike trains, *IEEE Eng. Med. Biol. Mag.* **13**, 197–202 (1994).

[35] M. C. Teich, R. G. Turcott, and R. M. Siegel, Variability and long-duration correlation in the sequence of action potentials in cat striate-cortex neurons, submitted to *IEEE Eng. Med. Biol. Mag.*, 1996.

[36] M. C. Teich, C. Heneghan, S. B. Lowen, T. Ozaki, and E. Kaplan, Fractal character of the neural spike train in the visual system of the cat, submitted to *J. Opt. Soc. Am. A*, 1996.

[37] J. B. Troy and J. G. Robson, Steady discharges of X and Y retinal ganglion cells of cat under photopic illuminance, *Visual Neurosci.* **9**, 535–553 (1992).

[38] R. G. Turcott and M. C. Teich, Long-duration correlation and attractor topology of the heartbeat rate differ for healthy patients and those with heart failure, *Proc. SPIE* **2036** (*Chaos in Biology and Medicine*), 22–39 (1993).

M. C. Teich, C. Heneghan, S. B. Lowen, and R. G. Turcott, in Wavelets in Medicine and Biology, edited by A. Aldroubi and M. Unser (CRC Press, Boca Raton, 1996), ch. 14, pp. 383-412.

[39] R. G. Turcott, P. D. R. Barker, and M. C. Teich, Long-duration correlation in the sequence of action potentials in an insect visual interneuron, *J. Stat. Comput. Simul.* **52**, 253–271 (1995).

[40] R. G. Turcott and M. C. Teich, Fractal character of the electrocardiogram: Distinguishing heart-failure and normal patients, *Ann. Biomed. Eng.* **24**, No. 2, 269–293 (1996).

[41] G. W. Wornell and A. V. Oppenheim, Estimation of fractal signals from noisy measurements using wavelets, *IEEE Trans. Sig. Process.* **40**, 611–623 (1992).